ADVANCED FUNCTIONAL MATERIALS
www.afm-journal.de

Unraveling the Atomic-scale Mechanism of Phase Transformations and Structural Evolutions during (de)Lithiation in Si Anodes

Fangjia Fu, Xiaoxu Wang, Linfeng Zhang, Yifang Yang, Jianhui Chen, Bo Xu, Chuying Ouyang, Shenzhen Xu,* Fu-Zhi Dai,* and Weinan E*

Unraveling the reaction paths and structural evolutions during charging/discharging processes are critical for the development and tailoring of silicon anodes for high-capacity batteries. However, a mechanistic understanding is still lacking due to the complex phase transformations between crystalline (c-) and amorphous (a-) phases involved in electrochemical cycles. In this study, by employing a newly developed machine learning potential, the key experimental phenomena not only reproduce, including voltage curves and structural evolution pathways, but also provide atomic scale mechanisms associated with these phenomena. The voltage plateaus of both the c-Si and a-Si lithiation processes are predicted with the plateau value difference close to experimental measurements, revealing the two-phase reaction mechanism and reaction path differences. The observed voltage hysteresis between lithiation and delithiation mainly originates from the transformation between the c-$Li_{15-\delta}Si_4$ and a-$Li_{15-\delta}Si_4$ phases. Furthermore, stress accumulation is simulated along different reaction paths, indicating a better cycling stability of the a-Si anode due to the lower stress concentration. Overall, the study provides a theoretical understanding of the thermodynamics of the complex structural evolutions in Si anodes during (de)lithiation processes, which may play a role in optimizations for battery performances.

1. Introduction

Silicon (Si), owing to its extremely high theoretical capacity (4200 mAh g^{-1} for $Li_{4.4}Si$), is regarded as one of the most attractive anode materials for next generation lithium batteries.[1,2] However, practical application of Si anode is severely hampered by its large volume expansion/shrinkage during lithiation/delithiation (discharging/charging). This expansion/shrinkage may give rise to anode particle pulverization, breaking the electrical contact between particles, and resulting in rapid capacity attenuation and limited cycle life.[1–5] The stress state of an anode particle depends strongly on the lithiation/delithiation mechanism. For example, McDowell et al.[6,7] pointed out that amorphous Si (a-Si) and crystalline Si (c-Si) have different stresses during lithiation. The stress distribution in a-Si particles is uniform and shows compressive hoop stress, which is beneficial to structural stability. In contrast, the core of c-Si is under compressive stress and

F. Fu, W. E
School of Mathematical Sciences
Peking University
Beijing 100871, China

F. Fu, L. Zhang, S. Xu, F.-Z. Dai, W. E
AI for Science Institute
Beijing 100084, China
E-mail: xushenzhen@pku.edu.cn; daifz@bjaisi.com

X. Wang, L. Zhang
DP Technology
Beijing 100080, China

Y. Yang, J. Chen, B. Xu, C. Ouyang
Fujian Science & Technology Innovation Laboratory for Energy Devices of China
Ningde 352100, China
E-mail: cyouyang@jxnu.edu.cn

B. Xu, C. Ouyang
Department of Physics
Laboratory of Computational Materials Physics
Jiangxi Normal University
Nanchang 330022, China

S. Xu
School of Materials Science and Engineering
Peking University
Beijing 100871, China

W. E
Center for Machine Learning Research
Peking University
Beijing 100871, China

The ORCID identification number(s) for the author(s) of this article can be found under https://doi.org/10.1002/adfm.202303936

DOI: 10.1002/adfm.202303936

the surface layer is under tensile stress, and this may lead to electrode cracks. For better development of Si anode, it is essential to understand the underlying mechanism of the lithiation/delithiation process and the corresponding microstructure evolution. However, the lithiation/delithiation of Si anode involves complex transitions between the crystalline and amorphous phases, making any comprehensive analysis a challenging task.

Experimental as well as theoretical efforts have been made in the past to understand the lithiation/delithiation of Si anode and to characterize the intermediate phases.[3,4,8] The general understanding on the lithiation/delithiation of Si anode can be summarized as follows:

1) During lithiation, c-Si phase transforms into amorphous Li_xSi (a-Li_xSi) phase, and finally converts into c-$Li_{15}Si_4$ phase at low voltages ≈50 mV versus Li/Li^+.[9–11] There are two clear voltage plateaus at ≈0.18 and 0.05 V versus Li/Li^+.[12]
2) During delithiation, the c-$Li_{15}Si_4$ phase converts back to a-Li_xSi phase, and then a-Si is formed after complete lithium removal. The a-Si never transforms back to c-Si.[11]
3) The lithiation of a-Si is similar to that of c-Si, except a deviation on the height of the first plateau.[10,11]
4) An evident voltage hysteresis (≈350 mV after the first cycle) is observed between the charging and discharging curves, indicating different reaction pathways of lithiation and delithiation.[13]

What remains unclear is the underlying atomic scale process behind these phenomena, e.g. the mechanism of the finite voltage hysteresis, the difference in the plateau height between a-Si and c-Si lithiation, the stress difference between a-Si and c-Si. These problems depend strongly on the lithiation/delithiation paths of Si anode, especially the structural evolution of crystalline to the intermediate a-Li_xSi phases. Even though considerable efforts have been made to study these issues,[14–24] there are still many controversies including the compositions and structure of the intermediate a-Li_xSi phases:

1) For the lithiation of c-Si, Dahn et al.[10] suggested that the intermediate phase was a-$Li_{3.5}Si$ by in situ X-ray diffraction (XRD). Grey et al.[14] reported that an a-Li_7Si_3 phase with distributed small Si clusters and Si-Si dumbbells was detected by XRD and ex situ nuclear magnetic resonance (NMR). Density functional theory (DFT) calculations revealed that the six-membered ring structure in c-Si was destroyed by the insertion of Li atoms, breaking the Si-Si network into smaller rings and chains with star and boomerang structures, and finally splitting into Si-Si dumbbells and isolated Si atoms.[15,17]
2) For the lithiation of a-Si, the a-Si phase transformed to a new amorphous phase (a-$Li_{2.5}Si$) via a two-phase mechanism as observed by transmission electron microscope (TEM).[18] The lithiation occurred extremely fast, making it impossible to obtain a series of other intermediate structures. In addition, in situ NMR showed that a-Si first converted into a-$Li_{2.0}Si$ and then converted into a-$Li_{3.5}Si$.[19] Theoretical study also suggested that a-$Li_{2.0}Si$ is a key structure, in which large Si clusters were transformed into small ones.[20] Yet other studies suggested that the intermediate phases were $Li_{2.17}Si$[21] or a-$Li_{2.9}Si$.[22]
3) For the delithiation of c-$Li_{15}Si_4$, XRD characterization revealed that the c-$Li_{15}Si_4$ phase was converted into a-$Li_{2.0}Si$.[10] Moreover, Car-Parrinello molecular dynamics (CPMD) calculation[23] suggested that a-$Li_{2.0}Si$ has lower amorphization energy than a-Li_3Si, and a-$Li_{2.0}Si$ as an important phase during electrochemical reaction. However, Grey et al.[14] proposed that the a-Si phase was directly formed by aggregation and growth of Si atoms when removing Li atoms, without any intermediate a-Li_xSi phases. Ogata et al.[19] classified c-$Li_{15}Si_4$ to over-lithiated c-$Li_{15+\delta}Si_4$ and Li-deficient c-$Li_{15-\delta}Si_4$ phases, and suggested c-$Li_{15-\delta}Si_4$ as the nucleus for Si clusters. The Si clusters grew through deleting Li, expanding the Si-Si network to form a-Si phase at a voltage higher than 0.3 V.

Molecular dynamics (MD) simulation is the main theoretical tool for studying the detailed lithiation/delithiation processes of Si anode.[20,25–27] However, the ability of MD simulations has traditionally been limited by the dilemma of accuracy and efficiency. Thanks to the development in the area of artificial intelligence, machine learning potentials[28,29] have made it possible to perform MD with ab initio accuracy for system sizes much larger than what was possible using traditional ab initio MD (AIMD).[15,17,22,23,30] This opens up a lot of new opportunities for efficiently simulating complex transition processes in battery material.[31–36] In the present work, we use deep potential (DP)[37,38] MD simulation to study the lithiation/delithiation processes of Si anode, evaluate reaction paths, characterize the microstructure evolution, and estimate the charging/discharging voltage curves. Our results reproduce the voltage plateau difference between c-Si and a-Si and the voltage hysteresis that have been observed in experiments. At the same time, they provide the atomic scale details of the two-phase process at the initial stage of the lithiation, and the difference of reaction paths between lithiation and delithiation. Thus, our results provide deep insights into the mechanism of lithiation/delithiation processes and the evolution of the electrochemical properties for the Si anode, which should be helpful for the further optimization of Si-anode materials.

2. Results and Discussion

2.1. Construction and Validation of the DP Model

The workflow for the construction of potential energy surface (PES) models by DP-Generator (DP-GEN)[39,40] and the calculations of corresponding electrochemical properties are illustrated in **Figure 1**. Computational details of constructing the DP model and the AIMD simulation are shown in Supporting Information (SI). First, we constructed and validated the DP model. We then applied the DP model to simulate electrochemical properties by the hybrid deep potential molecular dynamics (DeePMD) and grand canonical Monte Carlo (GCMC) method.[41]

The Li-Si DP model is validated by its accuracy in describing the energies, forces and structures, which are critical to reproducing the lithiation/delithiation processes of Si anode. **Figure 2**a,b compares the energies and forces of the DP model

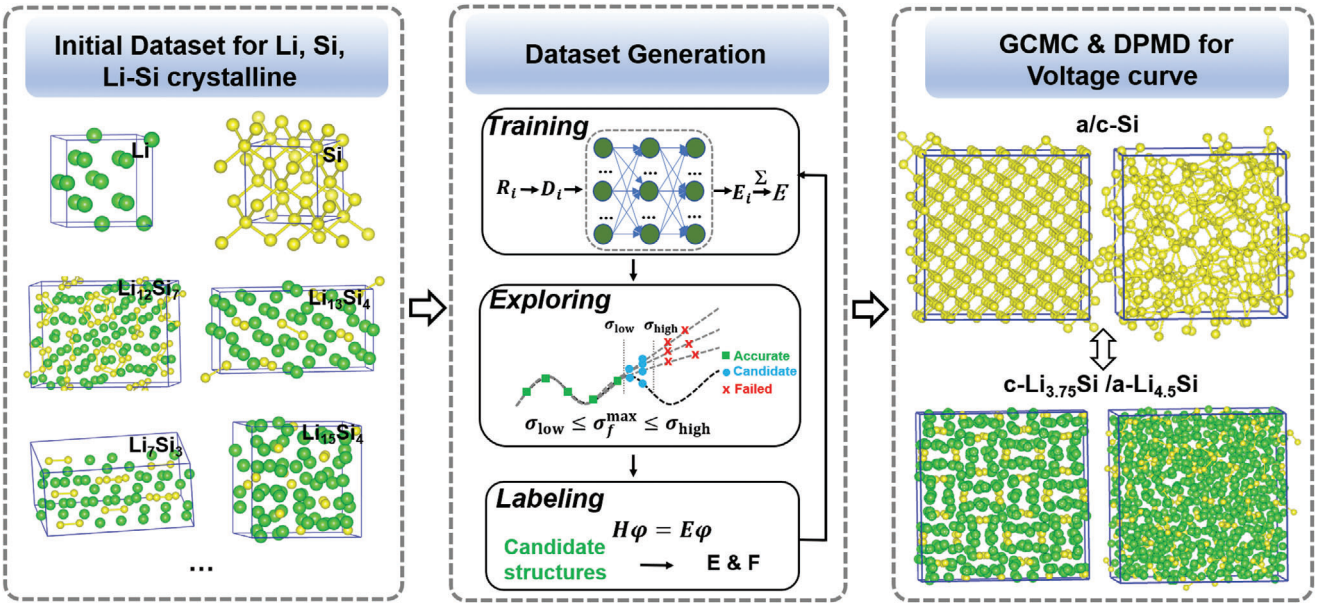

Figure 1. The workflow for constructing the deep potential model using the deep potential generator (DP-GEN) and applying the DP model to simulate the electrochemical property evolution during lithiation/delithiation. The green and yellow balls represent Li and Si atoms, respectively.

with DFT calculations for c-Li_xSi, a-Li_xSi, Li and Si systems. We can see that good agreement for energies and forces is achieved over a broad range of Li-Si compositions and structures, including crystalline and amorphous Li, Si, and Li_xSi. The root mean square error (RMSE) of energy of c-Li_xSi and a-Li_xSi is 0.015 and 0.008 eV atom^{-1}, respectively. The force RMSE of c-Li_xSi and a-Li_xSi is 0.119 and 0.170 eV Å^{-1}, respectively. Besides, an independent testing dataset is also constructed to validate the accuracy of DP model (see Supporting Information for configurations generation), and the RMSE of a-Li_xSi of energy and force is 0.007 eV atom^{-1} and 0.105 eV Å^{-1}, respectively.

Figure 2c–f compares the radial distribution functions (RDFs) of Li-Si pairs for various a-Li_xSi phases between AIMD (see Supporting Information for more details of the AIMD settings) and DeePMD. The RDFs of Li-Li pairs and Si-Si pairs are shown in Figure S1a, S1b (Supporting Information), and those RDF comparisons for the c-$Li_{15}Si_4$ phase are shown in Figure S1c (Supporting Information). The simulation boxes of a-Li_1Si_1, a-$Li_{12}Si_7$, a-$Li_{15}Si_4$, and a-$Li_{22}Si_5$ contain 512, 304, 608, and 432 atoms, respectively. It should be noted that four a-Li_xSi phases are random generated by DeePMD simulation. The RDF describes the spatial correlation and local bonding information of a material's structure. The characterization of amorphous phases can be assigned to a broad distribution of RDF profiles with respect to atoms' distances. As shown in Figure 2c–f; Figure S1 (Supporting Information), the RDF curves of DeePMD and AIMD match well with each other, indicating the reliability of the DP model in describing the structures of Li-Si phases. In addition, comparisons of lattice parameters between the DP model and DFT calculations are listed in Table S1 (Supporting Information), where the error is in the range of 0.07%–0.45%. These agreements guarantee reliable simulation results of the lithiation/delitheation processes in the Si anode.

2.2. Formation Energy and Voltage Curve

The formation energy is defined as:[8,42]

$$E_f\ (x) = E_{Li_xSi} - xE_{Li} - E_{Si} \quad (1)$$

where x is the number of Li atoms per Si atom, E_f is the formation energy per Si atom of c-Li_xSi/a-Li_xSi (unit: eV/Si atom). E_{Li_xSi} is the total energy per Si atom of c-Li_xSi/a-Li_xSi, E_{Li}, and E_{Si} are the total energies of BCC Li and amorphous Si per atom, respectively. Here, the energy of the most stable c-Si phase before lithiation is taken as the reference energy used for calculating formation energy.

For the lithiation/delithiation processes, the voltage relative to Li/Li^+ can be expressed as follows:[8,42]

$$V = -\frac{1}{e}\frac{E_f(x_2) - E_f(x_1)}{x_2 - x_1} \quad (2)$$

where e is the charge of the electron, and the unit is in volt (V).

The predicted formation energies and voltage curve of crystalline Li-Si phases by the DP model are compared with the experimental results, as shown in Figure S2 (Supporting Information). First, it should be noted that the DP results of voltage values are in good agreement with the DFT calculations for the thermodynamically stable phases of crystalline Li-Si, as demonstrated in Figure S2b (Supporting Information). It means that our DP force field is of the same accuracy level with DFT calculations. Secondly, there is a small voltage difference (only ≈0.07 V) between the DFT and experimental voltages. This deviation can be attributed to two factors:[17,31,43] one is the intrinsic error of DFT, the other is the ignorance of the entropy effect. However, these two factors are not relevant to the accuracy of our DP force field training. The deviation in entropic effect[17,43] is ≈0.06 V, which

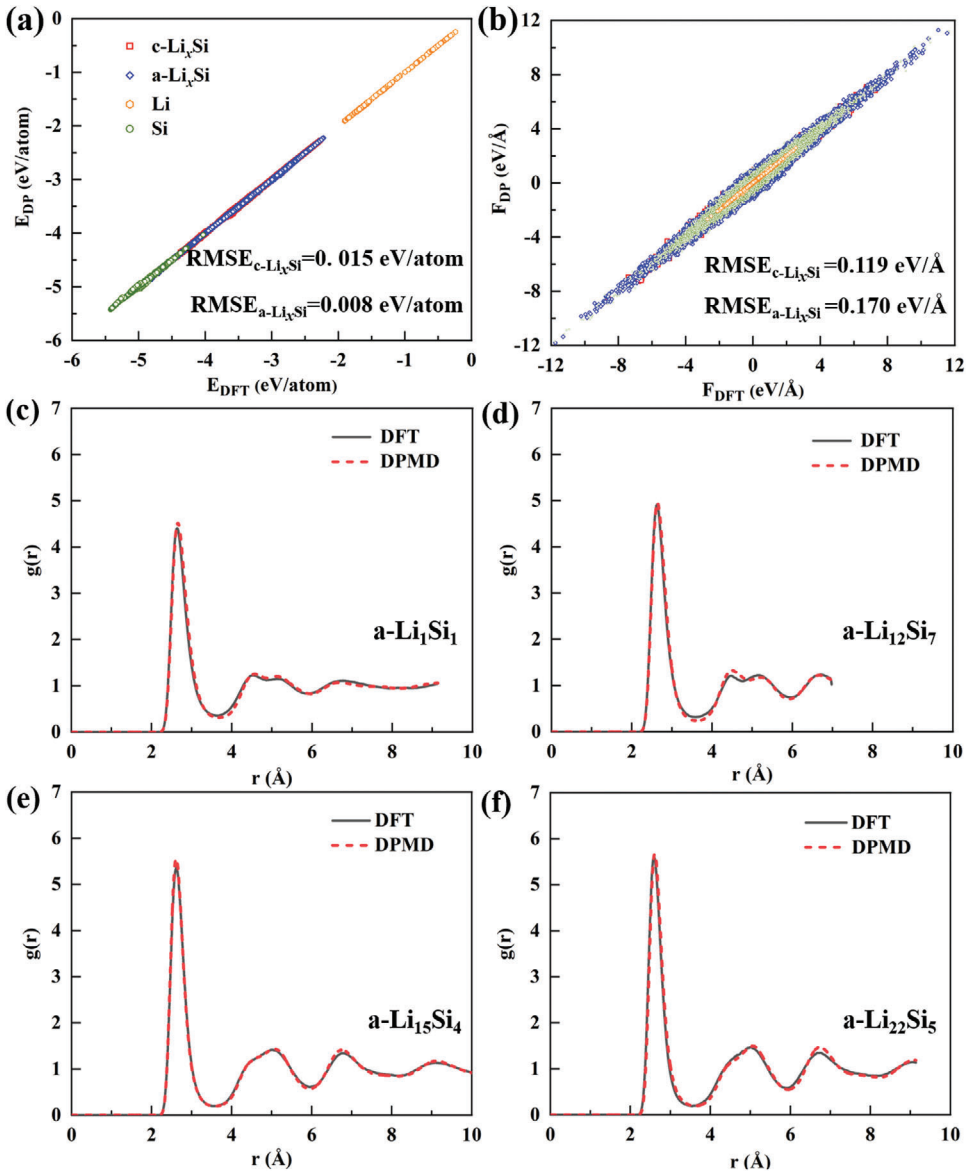

Figure 2. a,b) Comparison between energies and forces predicted by the DP model and those calculated by DFT. Crystalline Li_xSi (red square), amorphous Li_xSi (blue diamond), Li (orange hexagon), and Si (green circle) systems are represented by different symbols. c–f) The comparison between the AIMD (black line) and the DeePMD (red dash) radial distribution functions (RDFs) at 298 K for Li-Si pairs in various amorphous Li-Si phases.

can be attributed the experimental temperature of 688 K, while the DFT voltages are calculated at 0 K. Since our DP force field is trained based on the DFT data, the DP accuracy can be guaranteed as long as the agreement between the DFT and DP predicted voltages is satisfactory. In addition, according to the formation energy formula, the formation energy is the relative energy with respect to Li and Si. Although there is a prediction error, it is guaranteed that our model can qualitatively and semi-quantitatively analyze the voltage curve.

The hybrid DeePMD and GCMC simulations are used to calculate the formation energies and voltage curves of the lithiation/delithiation processes. Four simulations are performed, i.e., the lithiation processes of c-Si/a-Si and delithiation processes of c-$Li_{3.75}Si$/a-$Li_{4.5}Si$. Please refer to Figure S3 (Supporting Information) for the detailed scheme of Li insertion in a-Si by DeePMD and GCMC. The number of Si atoms is 216 for c-Si/a-Si, a-$Li_{4.5}Si$, and 128 for c-$Li_{3.75}Si$, and is fixed during the simulations. The number of Si depends on the supercell size of either c-Si or c-$Li_{3.75}Si$. The starting a-Si structure is obtained by melting the c-Si at 2500 K and annealing down to room temperature. The starting a-$Li_{4.5}Si$ structure is obtained by lithiation of c-Si. For convenience, the lithium intercalation processes based on c-Si and a-Si structures are defined as lithiation-c (L-c) and lithiation-a (L-a), and the lithium removal processes based on c-$Li_{3.75}Si$ and a-$Li_{4.5}Si$ structures are defined as delithiation-c (D-c) and delithiation-a (D-a), respectively.

The formation energies are calculated according to equation (1) based on the selected lowest energy structure of each

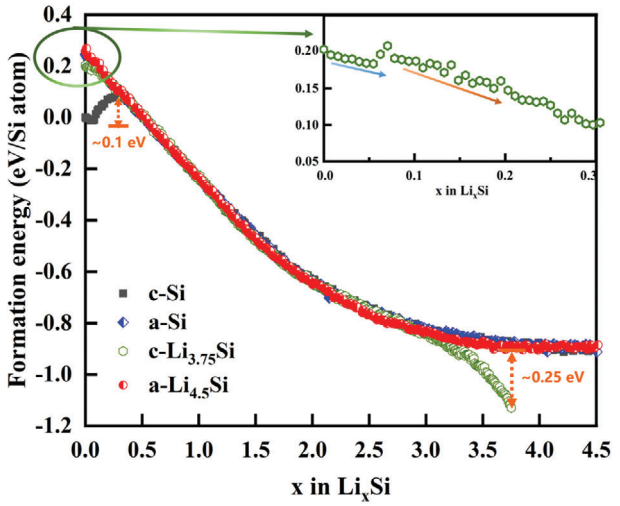

Figure 3. Formation energy (eV/Si atom) during lithiation and delithiation processes simulated by the hybrid DeePMD and GCMC method. The inset illustration shows the formation energies in the range of $0<x<0.3$ for c-$Li_{3.75}Si$ delithiation. The black squares and blue diamonds represent the lithiation of c-Si and a-Si with 216 atoms, respectively, the green hexagons represent the delithiation of c-$Li_{3.75}Si$ with 608 atoms (128 Si atoms), the red circles represent the delithiation of a-$Li_{4.5}Si$ with 1203 atoms (216 Si atoms).

composition. **Figure 3** shows the simulated formation energy curves, where different curves almost overlap with each other, indicating similar intermediate a-Li_xSi structures. The agreement between different curves means that the a-Li_xSi phases may reach their lowest energy and be meta-stable structures, since their starting structures and simulation processes are different. Roughly speaking, the formation energy first decreases linearly with the increase of Li when $x<2$, then the decreasing speed decreases when $2<x<3$, and finally the curve approaches a plateau when $x>3$. The initial stage of the lithiation/delithiation curve starting from a crystalline phase does not follow this tendency. In the initial stage of L-c ($x\approx0$) and D-c ($x\approx3.75$), corresponding to inserting Li into c-Si and removing Li from c-$Li_{3.75}Si$, the crystalline phase breaks and the a-Li_xSi phase forms, resulting in an abrupt energy jump. The corresponding energy jump of L-c and D-c are 0.1 and 0.25 eV, respectively. The value of energy jump in the L-c and D-c as shown in Figure 3 is defined as the jumping height. The magnitude of the abrupt energy jump is related to the latent heat of the structural transformation. For example, the formation energy difference between c-$Li_{3.75}Si$ and a-$Li_{3.75}Si$ is 0.27 eV, similar to the jumping height of D-c. The close proximity between the latent heat of c-$Li_{3.75}Si \rightarrow$ a-$Li_{3.75}Si$ transformation and the jumping height is due to the plateau-like shape of the formation energy curve when $x>3$.

We next turn to the detailed local shape of the formation energy curve. As shown in the enlarged part of the D-c curve with $x<0.3$, the formation energy suddenly increases by a small value at $x\approx0.06$ (see the arrows in the illustration in Figure 3). Though less obvious, this phenomenon also exists in L-c, L-a, and D-a curves. This sudden increase corresponds to the change from the stable solid solution of Li in Si to a-Li_xSi phase, and the corresponding snapshot can be seen in the initial stage of L-c reported in the section below. Therefore, the simulations broadly capture the lithiation/delithiation processes of Si anode, and we obtain a series of relaxed meta-stable amorphous structures.

The voltage curve reflects the battery performances and is one of the most fundamental electrochemical properties. The experimental studies[13,44] show that the deviation of the first voltage plateau between c-Si and a-Si is due to the different phase transformation paths, resulting in a thermodynamic voltage hysteresis. Different phase transformation paths between lithiation and delithiation processes can also bring about large thermodynamics hysteresis.[13,45] Besides, there are two main kinetics factors that also affect the structural transformations and thus give rise a hysteresis for voltage curve. One factor is the electrode and concentration polarization, a higher charging rate leads to a larger hysteresis loop.[44] Another factor is ohmic polarization, when the charging/discharging rate is very close to zero, the voltage curve still has a slight hysteresis loop due to the impedance effect.[46] This part of energy loss for kinetic hysteresis cannot be included in the simulations. It means that the GCMC simulation is employed to equilibrium structures in thermodynamics and further explore the voltage curve and phase transformation path.

Figure 4 shows the calculated voltage curves compared with experimental results from references.[19,45,47] The detailed explanations of the voltage curve calculations for the c-Si/a-Si lithiation and c-$Li_{3.75}Si$/a-$Li_{4.5}Si$ delithiation processes should be provided. First, we obtain the corresponding convex hull curves from all of the formation-energy data points during lithiation and delithiation processes, as shown in Figure S4 (Supporting Information). It notes that the convex hull is a plot of formation energies with respect to materials' compositions, in which envelopes connect the lowest-energy (or the thermodynamically stable) phases. The phases above the envelopes are either metastable or unstable. Secondly, the slope of each line segment connecting adjacent points in the convex hull curve corresponds to a voltage value, which is obtained from the equation (2). The voltage value between two adjacent Li contents, x_1 and x_2, can be plotted as a voltage plateau as displayed in Figure 4b–d.

For lithiation, the predicted voltage curves (Figure 4b) agree well with experimental results (Figure 4a). With the increase of Li content x, the lithiation voltage curve jumps abruptly from a high voltage to a stable plateau, and then the voltage decreases slowly to zero. The abrupt jump of the voltage curve is associated with the solid solution of Li in c-Si or a-Si. The plateau region is associated with the two-phase process. One phase is the c-Si or a-Si phase, while the other is a-Li_xSi phase. The c-Si or a-Si phase and the a-Li_xSi phase are two stable phases at the initial stage of the lithiation, which can be obtained in the formation energy curve. As displayed in Figure 4a,b, our results exhibit two-phase coexistence indicated by the voltage plateau in L-c or L-a. The simulation result not only reproduces the experimental voltage curve, but also agrees well with experimental observations by TEM.[6,18,24] As reported by McDowell and Liu et al.,[6,24] the initial lithiation mechanism of either c-Si or a-Si should follow a two-phase process. Furthermore, the plateau height difference of the lithiation between c-Si and a-Si is also well reproduced by our simulation. In experiments, the plateau of a-Si is 0.22 V higher compared to that of the c-Si case, while it is 0.17 V higher in the simulation. This voltage-plateau difference can be attributed to the fact that the initial Li intercalation formation energy of the

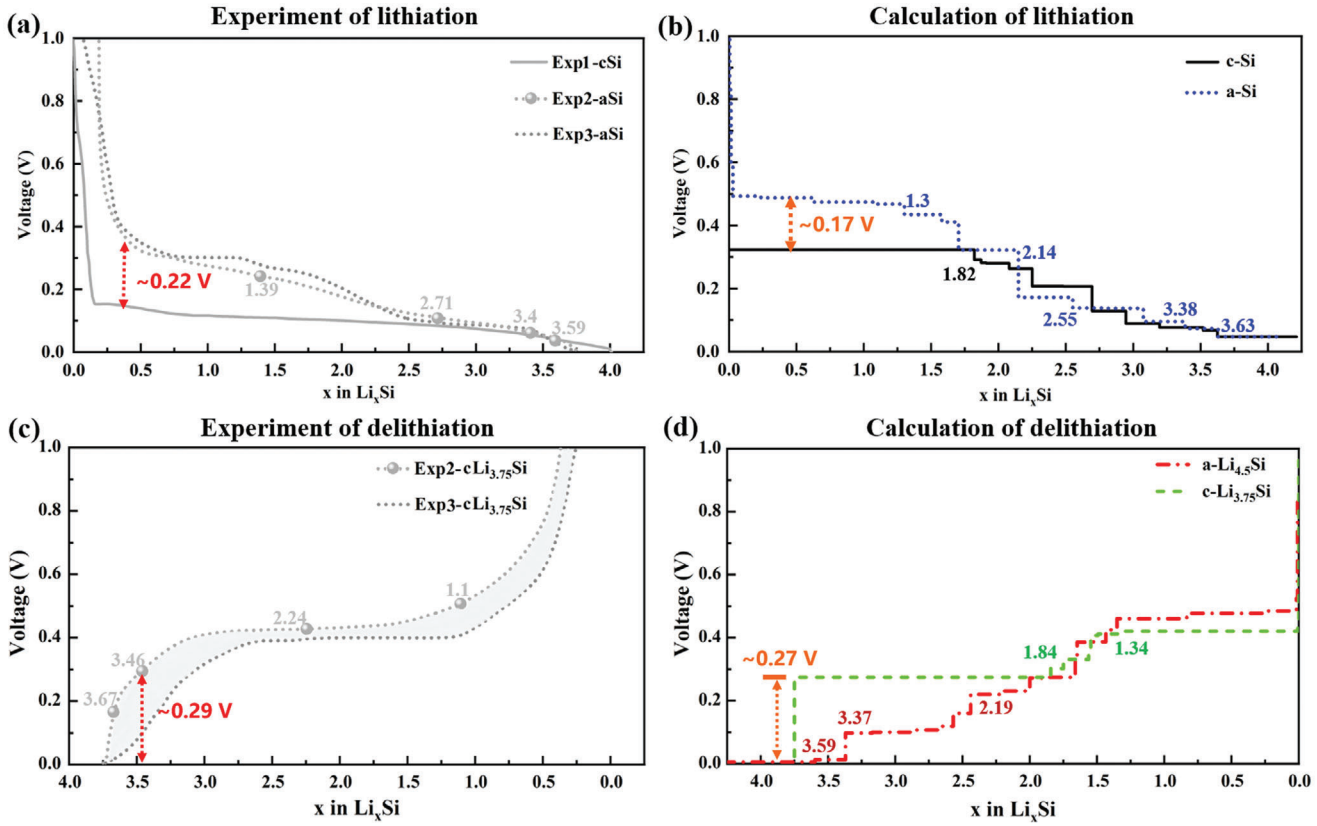

Figure 4. Comparison of the experimental and simulated voltage curves during lithiation and delithiation processes. a) Three experimental lithiation voltage curves of c-Si[47] and a-Si.[19,45] b) Simulated lithiation voltage curves of c-Si (black square) and a-Si (blue diamond). c) Two experimental delithiation voltage curves of c-$Li_{15}Si_4$.[19,45] d) Simulated delithiation voltage curves of c-$Li_{3.75}Si$ with 608 atoms and a-$Li_{4.5}Si$ with 1203 atoms. The numbers associated with the experimental and calculated voltage curves represent the lithium content ratio of x per Si. Each voltage plateau in DP calculations corresponds to the slope of each line segment connecting adjacent points in the convex hull curve.

c-Si (when x is approximately zero in c-Li_xSi) is lower than that of the a-Si, and both of the c-Si and the a-Si are connected to the same a-Li_xSi phase in the two-phase region. Therefore, as shown in the formation energy results (Figure 3), the phase with a higher Li insertion formation energy at the Li content $x \approx 0$ would exhibit a larger slope when connected to the endmember phase a-Li_xSi in the two-phase region, leading to a higher voltage plateau of the a-Si path. The predicted end point of the voltage plateau for L-c and L-a are ≈1.82 and 1.70 (see Figure 4b), respectively. The end point of L-c is derived based on the equilibrium a-Li_xSi with c-Si, while it is the end point of the linear part in the formation energy curve.

For delithiation, Figure 4c shows two experimental delithiation voltage curves of c-$Li_{3.75}Si$, while Figure 4d displays simulated delithiation voltage curves of c-$Li_{3.75}Si$ and a-$Li_{4.5}Si$. The delithiation voltage curve of a-$Li_{4.5}Si$ is similar to the lithiation voltage curve of a-Si, since their formation energy curves almost coincide with each other. The voltage first increases continuously with Li removal, then reaches a plateau value, and finally jumps abruptly to a high voltage value. However, the delithiation voltage curve of a-$Li_{4.5}Si$ is different from the experimental results, since their starting states are different. Nevertheless, when starting from c-$Li_{3.75}Si$, the simulated delithiation voltage curve is consistent with experimental results. The curve first abruptly becomes a plateau value with only a constant voltage value, and then increases with respect to removing Li, where the increasing speed also increases with Li removal. This constant voltage value of c-$Li_{3.75}Si$ in D-c is higher than that of amorphous phases in D-a within the Li content range of $1.84 < x < 3.75$, because the energy of the crystalline phase is lower and more stable. The latent heat associated with the transformation from the c-$Li_{3.75}Si$ phase to the amorphous phase is estimated as 0.27 V. This transformation results in irreversible energy loss, and leads to hysteresis in voltage curves.

In addition, we calculated the volume changes $((V_{Li_xSi} - V_{Si}) / V_{Si})/100$ of those lithiation and delithiation processes, as listed in Figure S5 (Supporting Information). It can be seen that the volume expansions predicted by the DP model are in good agreement with the experimental values[18] of purple balls for various Li_xSi phases. While there is a deviation of about 10%–30% from the experimental volume-expansion value[48] of the orange star. Obviously, there is a range for the volume expansion ratio in experimental results. Our model reproduces a volume expansion range from 270% to 290% (L-c: 291%, L-a: 283%, D-c: 270% and D-a: 285%) for the several Li_xSi phases (at $x = 3.75$). The computed volume changes in the four processes are also match well with the result of the atomic force microscope (AFM).[49] It should be noted that volume changes in AFM characterization starts from about 40% in the

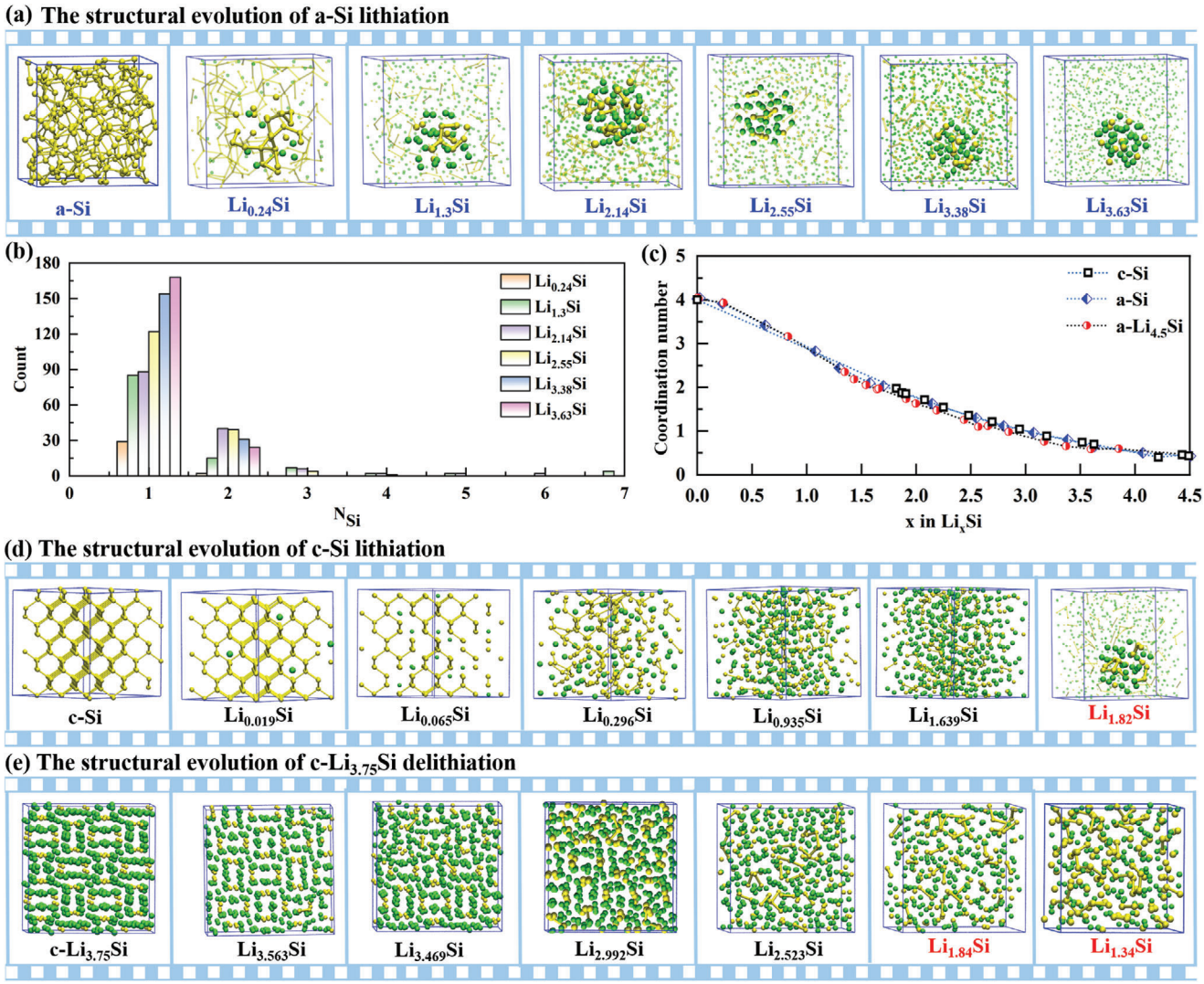

Figure 5. a) Typical snapshots of the amorphous lithiation process from a-Si to $Li_{3.63}Si$. Some atoms of various a-Li_xSi are highlighted to show the bonding architecture of Si ($r \leq 2.40$ Å). b) Comparison of the number of Si clusters for different Si atoms (N_{Si}, $r \leq 2.40$ Å) of various a-Li_xSi structures in a-Si lithiation. c) The average Si–Si coordination numbers versus the Li content of a/c-Si and a-$Li_{4.5}Si$ systems in the first coordination shell with a cutoff radius of 2.98 Å. d) Typical snapshots of the crystalline lithiation process from c-Si to $Li_{1.82}Si$. e) Typical snapshots of amorphous delithiation process from c-$Li_{3.75}Si$ to $Li_{1.34}Si$. The green and yellow balls represent Li and Si atoms, respectively.

second and third charging/discharging cycles due to the first cycle having a large deviation. Thus, the start point of volume change in AFM characterization has been re-zeroed in Figure S5 (Supporting Information). Those results also suggest that the sampled amorphous structures and computational properties are reliable.

2.3. Structural Evolution

The formation energies and voltage curves depend on the microstructural evolution during the processes of lithiation/delithiation. The structural evolution of lithiation from a-Si is shown in **Figure 5**a,b shows the variation of Si cluster with respect to the Li content *x*, and Figure 5c shows the coordination number of Si-Si as a function of *x*. It should be noticed from Figure 5a–c that the Si–Si bonds in a–Si structure gradually breakup during lithiation, from large Si clusters ($Li_{0.24}Si$) to ring-shaped and Y-shaped ($Li_{1.3}Si$) clusters, then to Si—Si dumbbells and to isolated Si atoms surrounded by multiple Li atoms ($Li_{2.55}Si$ and $Li_{3.38}Si$). The corresponding average coordination number of Si—Si goes from 3.8 to 0.5. The simulated results agree with experimental measurements. For example, the structure of a-$Li_{2.55}Si$ is similar to the $Li_{2.33}Si$ characterized by XRD,[14] which contains Si-Si dumbbells and isolated Si atoms, and the average coordination number of Si—Si is ≈1.5. The structure of a-$Li_{3.62}Si$ with 67 mV is similar to that of a-$Li_{3.4}Si$ with 60 mV reported by Grey and Ogata et al..[14,19] The a-$Li_{3.62}Si$ contains isolated Si and a few Si–Si bonds (see Figure 5b), and its Si–Si coordination number is 0.5 (see Figure 5c). It can be seen from Figure S6 (Supporting Information) that the Si bond distribution and corresponding Si/Si—Si clusters number of a-$Li_{2.33}Si$ and

a-$Li_{3.4}Si$ structures during the a–Si lithiation process are also similar to the Si bond distribution and Si/Si–Si clusters number of a-$Li_{2.55}Si$ and a-$Li_{3.62}Si$ structures. This means that the Si bond distribution of a-Li_xSi structures in a certain range are similar. Thus, we consider that the simulation has captured the whole lithiation process of a-Si.

The lithiation/delithiation structures starting from the crystalline phases are different from those starting from the amorphous phases, especially at the initial stage. Figure 5d indicates the structure changes of lithiation from c-Si to a-$Li_{1.82}Si$, while Figure 5e indicates the structure changes of delithiation from c-$Li_{3.75}Si$ to a-$Li_{1.34}Si$. The x range is chosen according to the voltage curves in Figure 4, where the lithiation/delithiation curves between the crystalline phases and the amorphous phases deviate from each other. At low Li concentration in L-c, the Li atoms in $Li_{0.019}Si$ are randomly inserted into the cavity of the Si cluster, and the Si tetrahedron framework remains unchanged, forming the solid solution of Li in Si. In $Li_{0.065}Si$ and $Li_{0.296}Si$, the Si–Si bond begins to break up and the long-range order gradually disappears. Subsequently the crystal transforms into the amorphous phase with distorted Si tetrahedrons. This is consistent with the fact that the formation energy of Li_xSi ($0<x<0.3$) structure gradually increases. For the Li_xSi ($x>0.3$) structure, they are completely amorphized. Analogously, it can be seen in D-c that the crystal gradually changes into an amorphous structure. The structure and shape of $Li_{3.469}Si$ with a few Li atoms removed remains unchanged, only a few Si–Si dimers appear. The Si–Si pairs become closer in $Li_{2.992}Si$, and the Si–Si–Si bonds appear with local disorder, but still maintain the crystalline phase. During the structural change from $Li_{2.523}Si$ to $Li_{1.34}Si$, Si gradually changes from isolated Si and Si–Si dumbbells to ring-shaped and Y-shaped Si clusters. There is a typical difference between L-c and D-c. Due to the limited solid solution content of Li in Si, the c-Si transforms rapidly to a-Li_xSi, leading to a two-phase transition mechanism during the initial lithiation and an abrupt jump in the voltage curve. In contrast, c-$Li_{3.75}Si$ transforms to a Li-deficient c-$Li_{15-\delta}Si_4$ during the initial delithiation stage and then becomes a-Li_xSi, as reported by Ogata et al..[19] Moreover, the voltage curve in Figure 4c shows that there is also a voltage plateau during delithiation starting from c-$Li_{3.75}Si$, indicating that c-$Li_{15}Si_4$ coexists another phase in this two-phase region. The a-$Li_{1.84}Si$ is the other endmember of this two-phase region as shown in Figure 4d, 5e. The voltage of the more stable c-$Li_{15}Si_4$ phase is higher than that of other amorphous phases in the Li content range of about $1.84<x<3.75$, which corresponds to the contribution of the latent heat of the phase transformation.

Using DeePMD and GCMC, we predicted the microstructure evolution paths of the crystalline and amorphous phases in the lithiation/delithiation processes. We see that the distributions of Li_xSi phases are consistent with earlier experimental results.

2.4. Stress Effect During Lithiation

The hybrid DeePMD and GCMC method was also employed to obtain the a-Li_xSi/Si binary-phase configurations by intercalating Li atoms into the central region of a c-Si or an a-Si supercell. During the simulations, a cubic box with ≈76 × 76 × 76 Å was adopted, and Li atoms were only inserted into the central 20 × 20 × 20 Å region. The insertion process was set to ≈25 Li atoms every 20 ps. As shown in **Figure 6**a, three representative configurations are selected to investigate the stress distribution. The conf1 and conf2 are picked from Li_{1308}/c-Si_{21952} and of Li_{1308}/a-Si_{21952}, which were obtained after lithiation by relaxing at 298 K for 10 ns in the isothermal-isobaric (NPT) ensemble. Conf3 is also picked from Li_{1308}/c-Si_{21952}, which was sampled by diffusing the Li atom of the conf1 at 1500 K with 100 ps. The starting structure of conf2 was obtained by melting the starting structure of conf1 at 2500 K. Stress sampling was carried out by running at 298 K for 100 ps. Those constructed configurations can be considered as the a-Li_xSi phases obtained after a quick or slow charging/discharging (high or low lithiation rate) process in experiments.[7] It should be mentioned that the lithiation process in experiments starts from the surface of Si nanoparticles and goes inward, resulting in the Li diffusion from the surface to the central region. While in our model, the Li insertion into Si materials originates from an inner region of the bulk Si systems. As an NPT condition (the pressure was set to be 1 bar and the cell's volume can be relaxed corresponding to this pressure) was adopted for this bulk Si model, when the simulation cell is relatively large (e.g., ≈22 K atoms in this DeePMD model), we assume the evolution of stress distribution around the Si/Li_xSi interface is approximately the same between our setup (Li insertion initiated at an inner region) and the experimental situation (Li insertion originating from the particle surface). In particular, for a certain position sufficiently far apart from the Li insertion region, it is difficult to tell the difference between the two distinct boundary conditions of Li insertion when the Si/Li_xSi heterogeneous interface approaches under an NPT ensemble condition. Thus, the bulk Li_xSi DP model in this work is employed to investigate the stress distribution in the heterogeneous Si/Li_xSi system, avoiding the extra expensive computational cost for training the DP models of the Si/vacuum and the Li_xSi/vacuum systems.

Experimental studies show that the internal stress will accumulate inside Si particles with Li insertion, the magnitude of which depends on the lithiation mechanism.[6,12,50] As shown above, combined with the evidences from earlier experiments, the initial lithiation of either c-Si or a-Si happens under a two-phase process condition. Thus, the a-Li_xSi/Si binary-phase is picked to study the stress distribution and the result is shown in Figure 6. Conf1 and conf3 of Li_{1308}/c-Si_{21952} and conf2 of Li_{1308}/a-Si_{21952} are selected to explore the stress distribution during lithiation. Starting from the structural cubic center, the range of $0<r\leq20.0$ Å is defined as the a-Li_xSi bulk region, $20.0<r\leq40.0$ Å is defined as the a-Li_xSi/c-Si or a-Li_xSi/a-Si interface region, and $r>40.0$ Å is defined as the c-Si or a-Si bulk region.

Figure 6b,c illustrate the stress distributions and atomic number density distributions of Li after lithiation. It can be seen that the distribution of Li is relatively uniform in a-Si in comparison with that of c-Si, as can be seen from Figure 6c. The relatively uniform distribution of Li renders a relatively uniform distribution of stress, as shown in Figure 6b, where one can see that the stress in a-Si is lower. The higher stress in the c-Si is caused by the lithiation process, indicating that Li insertion is less favorable thermodynamically at the beginning of charging for the c-Si case, and the derivative of the Li intercalation formation

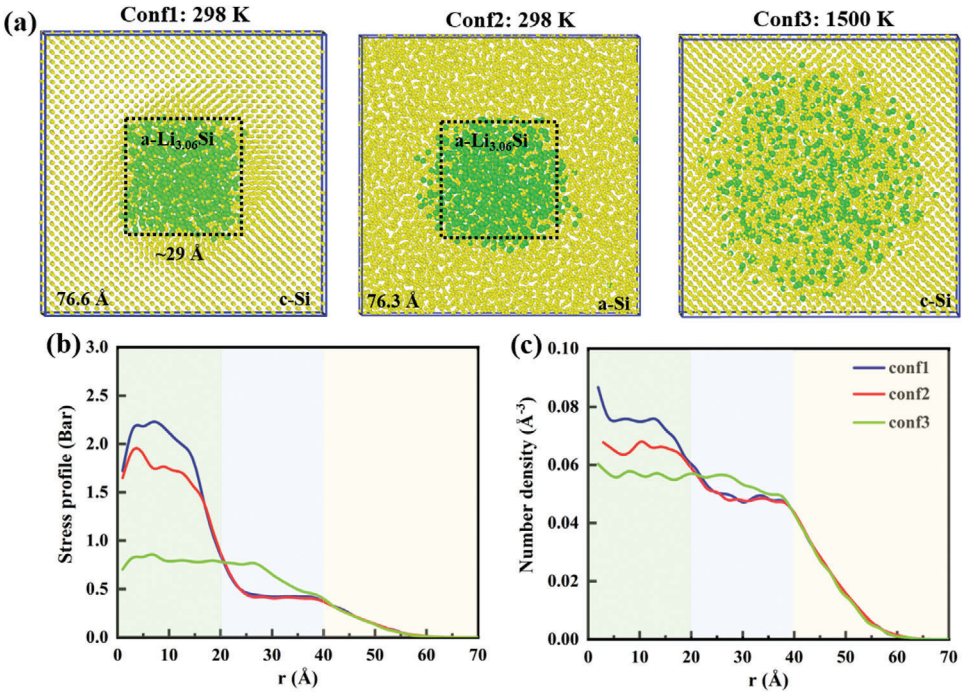

Figure 6. a) Cross-sectional schematic diagram of the configurations after the lithiation of crystalline Si (c-Si) and amorphous Si (a-Si) with 1308 Li atoms, respectively. Conf1 and conf3 are Li_{1308}/c-Si_{21952}, and conf2 is Li_{1308}/a-Si_{21952} at 298 K respectively. The starting a-Si of conf2 is obtained by melting the starting structure of conf1 at 2500 K, and conf3 is obtained by diffusing the Li atom in conf1 at 1500 K with 100 ps. b) The stress (Bar) and c) number density profile ($Å^{-3}$) for conf1, conf2, and conf3 at 298 K with 100 ps.

energy with respect to the Li content becomes more positive (see Figure 3) compared to the a-Si case, which leads to the difference of voltage plateaus between the c-Si and a-Si systems as shown in Figure 4. To further illustrate the effect of Li distribution on the stress distribution, we ran conf1 at 1500 K for 100 ps to obtain conf3, where Li diffuses to a more uniform distribution. As can be seen from Figure 6, the Li distribution is more uniform after diffusion, resulting in a significant reduction in stress concentration. The a-Li_xSi associated with the plateaus of a-Si has lower Li concentration, which further lead to lower stress in a-Si anodes in comparison to c-Si during lithiation. The results reveal that amorphous Si anode may exhibit better resistance to fracture, and increasing the Li diffusivity, e.g. nanominiaturization, may be a good approach to improve the performance and stability of Si anode. Except for the stress level, the strength and localized stress concentration are also important for the fracture of a particle, which are hard to obtain from either experiment or simulation. Nevertheless, experiments have revealed that the critical radius at which crack forms during lithiation of a-Si is much larger than that of c-Si, where it is ≈150 nm for c-Si and > 800 nm for a-Si.[3,6,50]

3. Discussion

The extreme volume change of Si electrodes during charging/discharging cycles has motivated researchers to investigate the reaction mechanism and structural evolutions of Si anodes, especially for the study of complex kinetics and thermodynamics for crystalline-to-amorphous and amorphous-to-amorphous phases transformation. For the theoretical study, one major challenge is to reproduce the voltage curves under different paths of lithiation and delithiation, and the other is to capture the structural evolution under different paths.

In this paper, the electrochemical properties of c-Si/a-Si lithiation and c-$Li_{3.75}$Si/a-$Li_{4.5}$Si delithiation processes are reproduced by using GCMC and DeePMD. Our simulations capture the qualitative features of the lithiation/delithiation processes of Si anodes, and we obtain a series of amorphous configurations in meta-stable states, providing comprehensive insights for the reaction mechanism under different charging/discharging paths. 1) In the process of c-Si/c-$Li_{3.75}$Si destruction and a-Li_xSi phases formation, the rapid jumps of formation energies and voltage curves are observed. The former corresponds to the transformation of crystal to the Li-Si solid solution and then to the a-Li_xSi phase, while the latter corresponds to the c-$Li_{15-\delta}Si_4$-like to the a-Li_xSi phases. The formation energy of c-$Li_{3.75}$Si to a-Li_xSi phase during Li removal (0.25 eV) is higher than that of c-Si to a-Li_xSi phase during Li insertion (0.10 eV). 2) The voltage plateaus in the initial stage of the c-Si and a-Si lithiation are reproduced by our simulations with a predicted voltage plateau difference of 0.17 V, which is comparable to the experimental value of 0.22 V. The successful prediction of the experimentally observed two-phase region in c-Si and a-Si is further justification for the computational scheme employed in this work. Different formation energy profiles of a/c-Si systems lead to different Li contents in the a-Li_xSi endmember of the two-phase region, which also matches well with previous experimental observations of the a-Li_xSi phase with different Li content.[10,14,18,19] 3) The simulation estimates that the latent heat from c-$Li_{3.75}$Si to a-$Li_{3.75}$Si phases is 0.27 V, which quantitatively agrees with experimental measurements. In

addition, the simulations show that there is a kinetic obstacle to converting a-$Li_{3.75}Si$ phase into c-$Li_{3.75}Si$ phase.

For the microstructure evolution pathways during lithiation/delithiation, our result reveals a series of intermediate a-Li_xSi phases that are consistent with experiments. During a-Si lithiation, the Si–Si bond breaks from large Si clusters to rings and Y clusters, then breaks into Si—Si dumbbells and isolated Si atoms. For example, the simulated a-$Li_{3.62}Si$ phase with 67 mV is similar to the experimental a-$Li_{3.4}Si$ with 60 mV.[14,19] During c-$Li_{3.75}Si$ delithiation, the structure remains unchanged with Li removal when $x>3.0$. The $Li_{2.992}Si$ also remains crystalline although some Si–Si dimers and Si–Si–Si bonds appear. This is similar to the Li-deficient c-$Li_{15-\delta}Si_4$ phase characterized by Ogata et al.,[19] which corresponds to the voltage jumps, but the structure remains unchanged in the range of $3.0<x<3.75$. During the c-Si lithiation, the Li-Si solid solution is initially formed in the low-Li region, and then the long-range order gradually disappears in the $Li_{0.296}Si$ phase and twists into amorphous Si tetrahedron. The first a-$Li_{1.82}Si$ phase captured by the corresponding voltage curve has a similar structure distribution to that of the Li_7Si_3 characterized by Grey et al.[14]

Stress simulations reveal that c-Si has higher stress than a-Si with Li insertion in the a-Li_xSi region. This can be attributed to the fact that Li intercalation into the crystalline Si phase is less favorable thermodynamically. Besides, the diffusion of Li atoms leads to stress homogenization, indicating that a-Si has better stability than c-Si.

4. Conclusion

In this work, we have trained a high-accuracy Li-Si deep potential covering the whole compositional space, and applied it to investigate the lithiation/delithiation processes of Si anode. DeePMD and GCMC are employed to simulate Li insertion/extraction, and to search for quasi-equilibrium intermediate a-Li_xSi structures from different starting structures, i.e., c-Si, a-Si, a-$Li_{4.5}Si$ and c-$Li_{3.75}Si$. Formation energies, voltage curves, and microstructure evolution pathways are calculated and analyzed based on the meta-stable intermediate a-Li_xSi structures. Our simulations agree well with experiments and reproduce several key experimental phenomena, for example, the voltage plateau and its difference between the lithiation of c-Si and a-Si and the hysteresis due to phase transformation from c-$Li_{15-\delta}Si_4$ to a-$Li_{15-\delta}Si_4$. In addition, our results provide rich insights into the lithiation/delithiation mechanisms of Si anodes, including the two-phase coexistence at the initial stage of lithiation, the difference of reaction paths between the lithiation and delithiation processes. We further studied the stress distribution of the lithiated c-Si and a-Si, and we saw that the stress magnitude in a-Si is lower than that in c-Si, indicating better resistance to fracture for the a-Si phase. Overall, our simulations provide a quantitative understanding of the lithiation/delithiation in Si anodes on atomic-scale mechanism, and it is hoped that it will be useful to design battery materials with better performance.

5. Experimental Section

Machine Learning: A DFT dataset covering a broad range of configurational space of Li-Si systems was necessary to train a DP model. A concurrent learning scheme, named DP-GEN,[39,40] was carried out to explore an extensive configuration space and collect the dataset for the DP model. The DP-GEN scheme runs in an iterative manner as shown in the middle panel of Figure 1. There were three subprocesses in each iteration:

1) Training. Four DP models with independent initializations of the network parameters were trained based on the existing dataset.
2) Exploration. Configurations were explored by DeePMD under NPT ensemble. To decide whether a new configuration encountered during the exploration should be labeled, the "model deviation" was used between the four models as the metric. The model deviation was defined as the maximal standard deviation of forces predicted by the four models σ_f^{max}. The configurations were categorized as "accurate", "candidate", and "fail" based on model deviations between the four models. Those configurations with $\sigma_f^{low} \le \sigma_f^{max} \le \sigma_f^{high}$ were classified as candidates.
3) Labeling. The configurations classified as candidates during exploration were randomly selected, labeled using DFT and then added to the dataset. The Vienna ab initio simulation package (VASP)[51,52] was employed for the DFT calculation.

Before the DP-GEN iterations, an initial dataset was generated by DFT calculations with some distorted structures, including the stable and metastable crystalline Li, Si and Li-Si phases from Materials Project.[53] After collecting the dataset, a productive DP model was trained, compressed,[54] and applied in subsequent simulations. The details of this construction were shown in the Supporting Information.

Simulation Methods: The LAMMPS package[55] complied with the DeePMD-kit package[37] was employed to do the simulations. Hybrid DeePMD and GCMC[41] method was used to simulate the lithiation processes of c-Si/a-Si and delithiation processes of c-$Li_{3.75}Si$/a-$Li_{4.5}Si$. The NPT ensemble was adopted during the simulations. For GCMC, one attempt of random Li insertion (the average number of exchange) and two attempts of random Li translation (the average number of move) every 1000 MD timesteps was performed. The total simulation time of a complete hybrid DeePMD and GCMC process was 10 ns for lithiation and delithiation, respectively. The time interval of a single MD step was 1 fs. After the hybrid simulations, the lowest energy configurations of each composition was picked. The configurations were then simulated by DeePMD under the NPT ensemble for another 5 ns with two attempts of random Li translation every 100 MD timesteps, and the structures were finally relaxed, on which further analysis of formation energies, voltage curves and atomic structures was investigated. In addition, the acceptance ratio in GCMC flow was 33.7% and 49.3% (a good target was between 20% and 50%)[41] for c-Si lithiation and c-$Li_{3.75}Si$ delithiation processes, respectively. Figure S7 (Supporting Information) shows that the formation energy curves with different acceptance ratio (different chemical potential) were similar to each other, indicating that the simulation results were converged. In addition, the formation energy of a-Li_xSi phases obtained from different processes were consistent with each other, which further confirms that quasi-equilibrium a-Li_xSi structures were guaranteed.

Supporting Information

Supporting Information is available from the Wiley Online Library or from the author.

Acknowledgements

This work gratefully acknowledges funding support from the Chinese Ministry of Science and Technology (Grant No. 2021YFB3800303), DP Technology Corporation (Grant No. 2021110016001141). C. O. and B. X. gratefully acknowledges the funding support from the National Natural Science Foundation of China (Grants No. 12174162, 51962010). The computing resource of this work was provided by the Bohrium Cloud Platform (https://bohrium.dp.tech), which was supported by DP Technology.

Conflict of Interest

The authors declare no conflict of interest.

Author Contributions

F.F., S.X., and F.Z.D. designed this project. F.F performed simulations and wrote the original manuscript. X.W. and L.Z. supported the machine learning training of potentials and data analysis. X.B. and C.O. supported and supervised the project. L.Z., C.O., S.X., F.Z.D. and W.E. helped to write and revise the manuscript. Y. Y. and J. C. assisted the GCMC simulations. All authors discussed the computational details and data analysis.

Data Availability Statement

The data that support the findings of this study are available from the corresponding author upon reasonable request.

Keywords

deep potential model, phase transformation, Si anodes, structural evolution, voltage curve

Received: April 9, 2023
Revised: April 24, 2023
Published online: May 24, 2023

[1] M. T. McDowell, S. W. Lee, W. D. Nix, Y. Cui, *Adv. Mater.* **2013**, *25*, 4966.
[2] M. N. Obrovac, V. L. Chevrier, *Chem. Rev.* **2014**, *114*, 11444.
[3] Z. L. Xu, X. Liu, Y. Luo, L. Zhou, J. K. Kim, *Prog. Mater. Sci.* **2017**, *90*, 1.
[4] M. Ge, C. Cao, G. M. Biesold, C. D. Sewell, S. M. Hao, J. Huang, W. Zhang, Y. Lai, Z. Lin, *Adv. Mater.* **2021**, *33*, 2004577.
[5] X. Zhao, V. P. Lehto, *Nanotechnology* **2021**, *32*, 042002.
[6] M. T. McDowell, S. W. Lee, J. T. Harris, B. A. Korgel, C. Wang, W. D. Nix, Y. Cui, *Nano Lett.* **2013**, *13*, 758.
[7] M. T. McDowell, S. Xia, T. Zhu, *Extrem. Mech. Lett.* **2016**, *9*, 480.
[8] Q. Zhang, Y. Cui, E. Wang, *Model. Simul. Mater. Sci. Eng.* **2013**, *21*, 074001.
[9] J. H. Ryu, J. W. Kim, Y. E. Sung, S. M. Oh, *Electrochem. Solid-State Lett.* **2004**, *7*, A306.
[10] J. Li, J. R. Dahn, *J. Electrochem. Soc.* **2007**, *154*, A156.
[11] M. N. Obrovac, L. J. Krause, *J. Electrochem. Soc.* **2007**, *154*, A103.
[12] M. Kim, Z. Yang, I. Bloom, *J. Electrochem. Soc.* **2021**, *168*, 010523.
[13] J. Lyubina, *Appl. Phys. Lett.* **2021**, *118*, 090501.
[14] B. Key, M. Morcrette, J. M. Tarascon, C. P. Grey, *J. Am. Chem. Soc.* **2011**, *133*, 503.
[15] P. Johari, Y. Qi, V. B. Shenoy, *Nano Lett.* **2011**, *11*, 5494.
[16] M. Gu, Z. Wang, J. G. Connell, D. E. Perea, L. J. Lauhon, F. Gao, C. Wang, *ACS Nano* **2013**, *7*, 6303.
[17] M. K. Y. Chan, C. Wolverton, J. P. Greeley, *J. Am. Chem. Soc.* **2012**, *134*, 14362.
[18] J. W. Wang, Y. He, F. Fan, X. H. Liu, S. Xia, Y. Liu, C. T. Harris, H. Li, J. Y. Huang, S. X. Mao, T. Zhu, *Nano Lett.* **2013**, *13*, 709.
[19] K. Ogata, E. Salager, C. J. Kerr, A. E. Fraser, C. Ducati, A. J. Morris, S. Hofmann, C. P. Grey, *Nat. Commun.* **2014**, *5*, 3217.
[20] E. D. Cubuk, E. Kaxiras, *Nano Lett.* **2014**, *14*, 4065.
[21] P. Limthongkul, Y.-I. Jang, N. J. Dudney, Y. M. Chiang, *Acta Mater.* **2003**, *51*, 1103.
[22] J. Danet, T. Brousse, K. Rasim, D. Guyomard, P. Moreau, *Phys. Chem. Chem. Phys.* **2010**, *12*, 220.
[23] K. S. Chan, W. W. Liang, C. K. Chan, *J. Phys. Chem. C* **2019**, *123*, 22775.
[24] X. H. Liu, J. W. Wang, S. Huang, F. Fan, X. Huang, Y. Liu, S. Krylyuk, J. Yoo, S. A. Dayeh, A. V. Davydov, S. X. Mao, S. T. Picraux, S. Zhang, J. Li, T. Zhu, J. Y. Huang, *Nat. Nanotechnol.* **2012**, *7*, 749.
[25] S. P. Kim, D. Datta, V. B. Shenoy, *J. Phys. Chem. C* **2014**, *118*, 17247.
[26] H. Jung, M. Lee, B. C. Yeo, K. R. Lee, S. S. Han, *J. Phys. Chem. C* **2015**, *119*, 3447.
[27] K. J. Kim, J. Wortman, S. Y. Kim, Y. Qi, *Nano Lett.* **2017**, *17*, 4330.
[28] V. L. Deringer, *J Phys Energy* **2020**, *2*, 041003.
[29] X. Chen, X. Liu, X. Shen, Q. Zhang, *Angew. Chem., Int. Ed.* **2021**, *60*, 2.
[30] H. Kim, C. Chou, J. G. Ekerdt, G. S. Hwang, *J. Phys. Chem. C* **2011**, *115*, 2514.
[31] N. Artrith, A. Urban, G. Ceder, *J. Chem. Phys.* **2018**, *148*, 241711.
[32] N. Xu, Y. Shi, Y. He, Q. Shao, *J. Phys. Chem. C* **2020**, *124*, 16278.
[33] L. Zhang, H. Wang, R. Car, E. Weinan, *Phys. Rev. Lett.* **2021**, *126*, 236001.
[34] J. Huang, L. Zhang, H. Wang, J. Zhao, J. Cheng, W. E, *J. Chem. Phys.* **2021**, *154*, 094703.
[35] G. H. Gu, J. Noh, I. Kim, Y. Jung, *J. Mater. Chem. A* **2019**, *7*, 17096.
[36] Z. Lu, *Rapp. Commun. - Colloq. Econ. Matiere Energ. Metall. Poudres* **2021**, *1*, 100047.
[37] H. Wang, L. Zhang, J. Han, W. E, *Comput. Phys. Commun.* **2018**, *228*, 178.
[38] L. Zhang, J. Han, H. Wang, R. Car, W. E, *Phys. Rev. Lett.* **2018**, *120*, 143001.
[39] L. Zhang, D. Y. Lin, H. Wang, R. Car, W. E, *Phys. Rev. Mater.* **2019**, *3*, 023804.
[40] Y. Zhang, H. Wang, W. Chen, J. Zeng, L. Zhang, H. Wang, W. E, *Comput. Phys. Commun.* **2020**, *253*, 107206.
[41] D. Frenkel, B. Smit, *Acad. Press. London* **2002**, 111.
[42] V. L. Chevrier, J. R. Dahn, *J. Electrochem. Soc.* **2009**, *156*, A454.
[43] V. L. Chevrier, J. W. Zwanziger, J. R. Dahn, *Can. J. Phys.* **2009**, *87*, 625.
[44] X. Zhang, X. Qiu, D. Kong, L. Zhou, Z. Li, X. Li, L. Zhi, *ACS Nano* **2017**, *11*, 7476.
[45] R. Chandrasekaran, A. Magasinski, G. Yushin, T. F. Fuller, *J. Electrochem. Soc.* **2010**, *157*, A1139.
[46] W. Dreyer, J. Jamnik, C. Guhlke, R. Huth, J. Moškon, M. Gaberšček, *Nat. Mater.* **2010**, *9*, 448.
[47] H. Wu, Y. Cui, *Nano Today* **2012**, *7*, 414.
[48] X. H. Liu, L. Q. Zhang, L. Zhong, Y. Liu, H. Zheng, J. W. Wang, J. H. Cho, S. A. Dayeh, S. T. Picraux, J. P. Sullivan, S. X. Mao, Z. Z. Ye, J. Y. Huang, *Nano Lett.* **2011**, *11*, 2251.
[49] L. Y. Beaulieu, T. D. Hatchard, A. Bonakdarpour, M. D. Fleischauer, J. R. Dahn, *J. Electrochem. Soc.* **2003**, *150*, A1457.
[50] X. H. Liu, L. Zhong, S. Huang, S. X. Mao, T. Zhu, J. Y. Huang, *ACS Nano* **2012**, *6*, 1522.
[51] G. Kresse, J. Furthmüller, *Phys. Rev. B* **1996**, *54*, 11169.
[52] G. Kresse, J. Furthmüller, *Comput. Mater. Sci.* **1996**, *6*, 15.
[53] A. Jain, S. P. Ong, G. Hautier, W. Chen, W. D. Richards, S. Dacek, S. Cholia, D. Gunter, D. Skinner, G. Ceder, K. A. Persson, *APL Mater.* **2013**, *1*, 011002.
[54] D. Lu, W. Jiang, Y. Chen, L. Zhang, W. Jia, H. Wang, M. Chen, *J. Chem. Theory Comput.* **2022**, *18*, 5559.
[55] S. Plimpton, *J Comput Phys* **1995**, *117*, 1.